J Nanopart Res (2016) 18:104
DOI 10.1007/s11051-016-3406-1

RESEARCH PAPER

# Superparamagnetic poly(methyl methacrylate) nanoparticles surface modified with folic acid presenting cell uptake mediated by endocytosis

**Paulo Emilio Feuser · Amanda Virtuoso Jacques · Juan Marcelo Carpio Arévalo · Maria Eliane Merlin Rocha · Maria Claudia dos Santos-Silva · Claudia Sayer · Pedro H. Hermes de Araújo**

Received: 27 October 2015 / Accepted: 26 March 2016 / Published online: 12 April 2016


**Abstract** The encapsulation of superparamagnetic nanoparticles (MNPs) in polymeric nanoparticles (NPs) with modified surfaces can improve targeted delivery and induce cell death by hyperthermia. The goals of this study were to synthesize and characterize surface modified superparamagnetic poly(methyl methacrylate) with folic acid (FA) prepared by miniemulsion polymerization (MNPsPMMA-FA) and to evaluate their in vitro cytotoxicity and cellular uptake in non-tumor cells, murine fibroblast (L929) cells and tumor cells that overexpressed folate receptor (FR) β, and chronic myeloid leukemia cells in blast crisis (K562). Lastly, hemolysis assays were performed on human red blood cells. MNPsPMMA-FA presented an average mean diameter of 135 nm and a saturation magnetization (Ms) value of 37 emu/g of iron oxide, as well as superparamagnetic behavior. The MNPsPMMA-FA did not present cytotoxicity in L929 and K562 cells. Cellular uptake assays showed a higher uptake of MNPsPMMA-FA than MNPsPMMA in K562 cells when incubated at 37 °C. On the other hand, MNPsPMMA-FA showed a low uptake when endocytosis mechanisms were blocked at low temperature (4 °C), suggesting that the MNPsPMMA-FA uptake was mediated by endocytosis. High concentrations of MNPsPMMA-FA showed hemocompatibility when incubated for 24 h in human red blood cells. Therefore, our results suggest that these carrier systems can be an excellent alternative in targeted drug delivery via FR.

**Keywords** Superparamagnetic · Nanoparticles · Poly(methyl methacrylate) · Folic acid · Cell uptake · Targetted drugs · Nanomedicine

P. E. Feuser · C. Sayer · P. H. H. de Araújo (✉)
Department of Chemical Engineering and Food Engineering, Federal University of Santa Catarina, Florianopolis, Brazil
e-mail: pedro.h.araujo@ufsc.br

A. V. Jacques · M. C. dos Santos-Silva
Department of Clinical Analyses, Federal University of Santa Catarina, Florianopolis, Brazil

J. M. C. Arévalo · M. E. M. Rocha
Department of Biochemistry and Molecular Biology, Federal University of Paraná, Curitiba, Brazil

## Introduction

Due to their unique physical properties, magnetic nanoparticles (MNPs), have been widely used in various biomedical applications, such as, targeted drug delivery (Zhao et al. 2013; Zheng et al. 2005), hyperthermia (Simioni et al. 2007; Kumar and Mohamad 2011; Feuser et al. 2015a), and magnetic resonance imaging (MRI) (Gupta and Gupta 2005; Abulateefeh et al. 2011). For these applications, MNPs must have combined properties of high magnetic saturation, superparamagnetic properties and biocompatibility (Zheng et al. 2005; Kumar and Mohamad

2011). MNPs represented by magnetite ($Fe_3O_4$) are often made in sizes smaller than 15 nm in diameter and their superparamagnetic properties are sufficient to cause tumor cell death by hyperthermia (Feuser et al. 2015a, b). However, the use of pure MNPs for these applications is challenging due to the high surface to volume ratio and strong dipole–dipole interaction between the particles, which makes MNPs agglomeration possible (Kumar et al. 2014; Tang et al. 2013). The agglomeration of MNPs can be attenuated with the encapsulation of MNPs in polymeric nanoparticles (NPs). The encapsulation of MNPs in polymeric NPs improves their chemical and physical stability, solubility, biological stability, target delivery and reduces the side effects of the encapsulated material (Fan et al. 2009; Zhang et al. 2011; Akbarzadeh et al. 2012). A large number of strategies have been proposed in the literature to encapsulate MNPs in polymeric colloidal particles including, inverse miniemulsion polymerization (Romio et al. 2013) and direct miniemulsion polymerization (He et al. 2009; Yan et al. 2011; Feuser et al. 2015a).

Polymeric NPs can be prepared from natural or synthetic polymers (Landfester and Mailander 2013). They have been studied extensively as drugs carriers, where the main advantages are the protection of the drug, controlled release and the possibility of drug delivery within the targeted cell or tissue (Feuser et al. 2016; Landfester and Musyanovych 2010; Landfester and Mailander 2013). Miniemulsion polymerization allows the production of polymeric NPs with unique characteristics of great interest for biomedical application, producing stable aqueous dispersions of droplets (50–500 nm) containing monomer, surfactant, ultrahydrophobe, initiator, and water-insoluble compounds (e.g., hydrophobic MNPs) by applying high shear stress (Higuchi and Mira 1962; Landfester 2009; Crespy and Landfester 2010; Asua 2014). The main advantage of the miniemulsion polymerization process is the ability to produce complex nanostructures, including inorganic nanoparticle encapsulation, in a single-reaction step with fast polymerization rates (Qiu et al. 2007; Mahdavian et al. 2008).

The NPs surface modification with folic acid (FA) can increase drug uptake in tumor cells that express high levels of type α or β folate receptors (FR). The FR-α is significantly overexpressed on the surface of tumor cells, while the FR-β is overexpressed in leukemic cells and macrophages. FRs exhibit limited expression on non-tumor cells and tissues, where one of the main advantages is the targeted drug delivery by folate receptors (Bhattacharya et al. 2007; Jia-Jyun et al. 2009; Wibowo et al. 2013; Yang et al. 2014; Lee et al. 2015). FR-mediated drug delivery is facilitated by endocytosis, which may enable drug delivery (Sudimack and Lee 2000; Pengcheng et al. 2013; Chen et al. 2013). The NPs can be internalized across a plasmatic membrane (passive diffusion) and through endocytosis (NPs are engulfed by endocytic vesicles) (Wang et al. 2012). Several in vitro studies have demonstrated that the modified surface of nanoparticles with FA increases the cellular uptake in tumor cells that overexpressed FR (Zhang et al. 2009; Duan et al. 2012; Sahoo et al. 2013; Yang et al. 2014). In vivo studies were also performed, as for instance by Arosio et al. (2015) who showed that NPs functionalized with FA increased the therapeutic efficacy of drugs due to the targeting ability and prolonged retention in breast tumor tissues. However, the functionalization or adsorption of the ligands cannot ensure drug delivery when it is intravenously administered (in vivo). When the functionalized nanoparticles enter the bloodstream they need to cross the blood vessel endothelial cells, which do not express FR, in order to reach the interstitial space of tumor sites (Chin and Ferreira 1999; Andhariya et al. 2013). To overcome this, a drug delivery system with superparamagnetic proprieties was proposed that could be attracted by external magnetic field (Mody et al. 2014) and uptake in vivo by FR mediated by endocytosis (Zheng et al. 2005; Xu and Su 2013). Chen et al. (2012) developed a nanoplatform for guided drug delivery by conjugation quantum dots with carbon nanotubes filled with $Fe_3O_4$. The authors demonstrated in vitro that this nanoplatform was capable to transport doxorubicin into HeLa cells by means of an external magnetic field. Chertok et al. (2008) showed in vivo that magnetic targeting induced a 5-fold increase accumulation of MNPs over non-targeted tumors. Furthermore, MNPs can also induce cell death by hyperthermia, when external alternating magnetic fields are applied (Xu et al. 2014, Mody et al. 2014; Feuser et al. 2015a, b). In a previous study, Feuser et al. (2015a) showed that superparamagnetic poly(methyl methacrylate) nanoparticles obtained by miniemulsion polymerization induced glioblastoma (U87MG) cell death when alternating magnetic fields were applied for 6 min.

The goal of this study was to synthesize and characterize superparamagnetic poly(methyl methacrylate) (PMMA) NPs obtained by miniemulsion polymerization surface modified with folic acid. In vitro cytotoxicity and cellular uptake assays were performed with the surface modified superparamagnetic poly(methyl methacrylate) (PMMA) with FA (MNPsPMMA-FA) and without FA (MNPsPMMA) on non-tumor cells, murine fibroblast cells (L929), cells that overexpressed FR-β, and chronic myeloid leukemia (K562) cells at two different temperatures (4 and 37 °C). Lastly, hemolysis assays were performed on human red blood cells.

## Experimental procedure

### Materials

For synthesis of magnetic nanoparticles coated with oleic acid (MNPsOA), the following reagents were used (high purity grade): ferrous sulfate ($FeSO_4 \cdot 4H_2O$), iron (III) chloride hexahydrate ($FeCl_3 \cdot 6H_2O$), ammonium hydroxide (99 %), and oleic acid (OA), all purchased from chemistry Vetec. For the preparation of surface modified superparamagnetic PMMA NPs with FA (MNPsPMMA-FA), the following reagents were used: methyl methacrylate (MMA) obtained from chemistry Arinos, azobisisobutyronitrile (AIBN) and folic acid (FA) purchased from chemistry Vetec, lecithin obtained from Alpha Aesar, and Crodamol GTCC (as co-stabilizer) purchased from Croda. Distilled water was used throughout the experiments.

## Methods

### Synthesis of MNPs(OA)

MNPs(OA) were prepared by co-precipitation in aqueous phase methods as described by Feuser et al. (2015a). Momentarily, $FeCl_3 \cdot 6H_2O$ and $FeSO_4 \cdot 7H_2O$ (mole ratio of 1:1.2) were dissolved in a beaker containing distilled water under mechanical stirring in the range of 800 rpm. Afterwards an ammonium hydroxide solution (11 mL) was rapidly added to the solution. After 1 h, 30 mL was added to the OA and the stirring process was continued (800 rpm) for 1 h. The MNPs(OA) produced was centrifuged and washed three times with ethanol to remove the unreacted OA.

### Preparation of MNPsPMMA-FA by miniemulsion polymerization

For encapsulation of MNPs(OA) by miniemulsion polymerization, an organic phase containing 2 g of MMA with 0.4 g of MNPs(OA), 0.1 g of lecithin, 0.1 g of crodamol, and 0.04 g of AIBN were added to a beaker containing 20 mL of distilled water and 0.02 g of FA (aqueous phase). The organic phase was added dropwise under higher shear with an amplitude of 70 % (Fisher Scientific, Sonic Dismembrator, 500 W). The high shear was maintained for 5 min (10 s on and 1 s off) in an ice bath immersed beaker to avoid an increased temperature during sonication. The miniemulsion product was transferred to glass tubes (10 mL) at 70 °C for polymerization during 3 h. Afterwards the material was cooled, centrifuged and washed three times with phosphate buffered saline (PBS) at pH 7.4. Subsequently, NPs were resuspended in 20 mL of PBS buffer. The magnetic fluid concentration used to produce the FA-MNPsPMMA was about $7 \times 10^{16}$ particles $mL^{-1}$. For a comparative study, PMMA NPs coated MNPs were prepared without folic acid (MNPsPMMA). The method of preparation was the same already described by Feuser et al. (2015a).

### Preparation of MNPsPMMA-FA by miniemulsion polymerization labeled with 6-coumarin

A highly fluorescent molecule, 6-coumarin, was dissolved in Miglyol to form a uniform solution (0.5 mg $mL^{-1}$). This solution (6-coumarin/crodamol) was used in the preparation of NPs to assess cellular uptake by fluorescence microscopy. In a beaker MNPs(OA) containing 20 mL of distilled water and 0.02 g of FA (aqueous phase) the organic phase was added (2 g of MMA with 0.4 g of MNPs(OA), 0.1 g of lecithin, 0.1 g of solution crodamol/6-coumarin and 0.04 g of AIBN) dropwise under higher shear (amplitude of 70 %). The following steps are the same as previously described.

### Characterization

Monomer consumption was monitored by gravimetric analysis of samples withdrawn from the polymerization medium at different times and the reaction was

stopped with addition of a 1 % hydroquinone (w/w) solution. The determination of the concentration of residual monomer after the polymerization reaction in miniemulsion was performed by GC (Shimadzu GC2010AF). Particle size and surface charge were measured by dynamic light scattering (DLS) using a Malvern Zetasizer Nano ZS analyzer. The NPs morphology was observed using a JEM 2100F transmission electron microscope (TEM) operating at 80 kV. Average particle size and polydispersity index (PdI) were also measured by dynamic light scattering and the surface charge of the NPs was investigated through zeta potential measurements (in both cases using the same Zetasizer). All samples were analyzed three times, from which the average and standard deviation (SD) were calculated. Chemical characterization was performed by Fourier transform infrared spectroscopy (FT-IR) using KBr pellets. X-ray diffraction (XRD) experiments were performed to identify the crystallographic structure of MNPs(OA) and MNPsPMMA-FA NPs. The crystalline phase of NPs was identified by XRD measurements using an XPert-Pro diffractometer, Cu-Kα (alpha) radiation (45 kV/40 mA) in the 2θ (theta) range of 20–80°. Thermogravimetric analysis (TGA) was performed. The MNPs(OA) and MNPsPMMA-FA NPs were measured through TGA runs under nitrogen atmosphere at a heating rate of 10 °C/min. A MicroSense model EV9 vibrating sample magnetometer (VSM) was used to measure the hysteresis loops of MNPs(OA) and MNPsPMMA-FA NPs. All analyses were performed at room temperature.

## In vitro studies

### *Cell culture and maintenance*

K562 cells were cultured in Roswell Park Memorial Institute Medium (RPMI) (GIBCO, São Paulo, SP, Brazil) supplemented with 10 % heat-inactivated fetal bovine serum (FBS), 100 U/mL penicillin, 100 μg $mL^{-1}$ streptomycin and 10 mM HEPES under 5 % $CO_2$ humidified atmosphere in 75 $cm^2$ flasks at 37 °C. Cell lines were purchased from American Type Culture Collection (ATCC, Rockville, MD, USA). L929 cells were cultured in Dulbecco's Modified Eagle's Medium (DMEM) (GIBCO, São Paulo, SP, Brazil) supplemented with 10 % heat-inactivated fetal bovine serum (FBS), 100 U/mL penicillin, 100 μg $mL^{-1}$streptomycin and 10 mM HEPES under 5 % $CO_2$ humidified atmosphere in 75 $cm^2$ flasks at 37 °C. Cell lines were purchased from American Type Culture Collection (ATCC, Rockville, MD, USA).

### *Viability assay (MTT assay)*

The MTT cell proliferation assay was employed to assess cell viability after the cytotoxic assay. Briefly, 150 μL of medium was removed and 50 μL $mL^{-1}$ of MTT solution (5 mg $mL^{-1}$) was added to each well. The cells were then incubated for 4 h, at 37 °C and 5 % $CO_2$ to allow the formazan-formation reaction. Following incubation, the medium containing the MTT solution was removed, and the formazan crystals were dissolved in 2-propanol. The optical density was measured at 570 and 690 nm using a *Safire2* microplate reader (Tecan Group Ltd.). The results are presented as survival percentage, where the control (untreated cells) was 100 %.

### *Cellular uptake by fluorescence microscopy*

The intracellular fate of carrier systems marked with 6-coumarin (MNPsPMMA and MNPsPMMA-FA) were evaluated with fluorescence microscopy. L929 and K562 cells were cultured at a density of $5 \times 10^5$ cells/mL, 200 mL/well. MNPsPMMA and MNPsPMMA-FA NPs were incubated at a low temperature (4 °C), blocking receptor-mediated endocytosis mechanisms (Leamon and Low 1991; García-Días et al. 2011), and at 37 °C with a concentration of 100 μg $mL^{-1}$. After 2 h of incubation, L929 and K562 cells were washed with PBS (*three times*) and the coverslips covering the bottom of the plate were removed and placed on a glass slide. Cell morphology and cellular uptake were evaluated by optical microscopy and the fluorescence of NPs was monitored by fluorescence microscopy. Cell images were acquired using emission mode with 20× objective after exciting the sample from 450 to 490 nm using barrier filters. Cells were observed under a fluorescence microscope (Olympus BX41) and representative fields were photographed with a digital camera. *Three different fields with cell homogeneity of the glass slide were measured and quantified by ImageJ software* (Collins 2007). *The experiments were performed in triplicate*. Fluorescence intensity was calculated as fluorescence intensity of the NPs divided by the fluorescence

intensity of control group (Dong et al. 2014). *The image background was subtracts by ImageJ software. Statistical analysis was performed using one-way ANOVA followed by post-test Bonferroni's.*

*Hemolysis assay*

In order to analyze the effect of MNPsPMMA-AF in normal red blood cells (RBC), five human blood samples were collected according to the ethics committee requirements (CEPSH no 913/2010). Briefly, 4 mL of whole blood was added to 8 mL of a sterile solution of sodium chloride in water (saline) and the RBCs were isolated from serum by centrifugation at 10,000×*g* for 5 min. The RBCs were further washed five times with saline solution; after that, the RBCs were diluted in 2 mL of saline. Then 120 μL of the diluted RBC suspension was added to 880 μL of water or saline. Samples were treated with MNPsPMMA-AF at a concentration of 50 and 100 μg $mL^{-1}$. All samples were prepared in triplicate and the suspension was briefly vortexed before undergoing a gentle stirring at 37 °C for 60 min. Afterwards, the mixture was briefly vortexed again and centrifuged at 10,000×*g* for 5 min. 100 μL of supernatant was transferred to a 96-well plate. The absorbance value of hemoglobin at 570 nm was measured with the reference wavelength at 540 nm. 120 μL of the diluted RBC suspension incubated with 880 μL of water and saline was used as the positive and negative control, respectively (Yu et al. 2011; Wang et al. 2009). Hemolysis percentage was calculated according to Eq. 1:

$$\text{Hemolysis}(\%) = \frac{\text{Sample absorbance} - \text{negative control}}{\text{Positive control} - \text{negative control}} \times 100 \quad (1)$$

## Results and discussion

The polymerization kinetics of NPs with and without FA obtained by miniemulsion polymerization was verified by gravimetric conversion. Analysis of residual monomer is an important parameter to be evaluated, since the total conversion of the monomer to polymer avoids possible toxic effects of the residual monomer, allowing application of the PMMA NPs in the biomedical field (Bettencourt and Almeida 2010; Gosavi et al. 2010). The gravimetric conversion presented in Fig. 1 showed that around 200 min of reaction the conversion of MNPsPMMA and MNPsPMMA-FA reached approximately 98 %. As shown in Fig. 1, the final conversion did not reach 100 %, probably due to the loss of monomer (MMA) by evaporation during the emulsification and polymerization stages. Monomer evaporation can occur due to high vapor pressure of the MMA (Feuser et al. 2016). It is important to mention that FA did not interfere in the polymerization rate.

The results of the DLS and TEM analyses are presented in Fig. 2. DLS analyses (Fig. 2a, c) showed that the MNPsPMMA and MNPsPMMA-FA NPs have intensity average particle diameters of 104 ± 3.9 nm and 134 ± 3.5 nm, and a polydispersity index of 0.11 ± 0.02 and 0.14 ± 0.02, respectively. The FA adsorption on NPs surface increased the average size by approximately 30 nm, when compared to NPs without FA. TEM images of MNPsPMMA-FA showed dark regions (black arrow) (Fig. 2b, d), which are attributed to the presence of MNPs (6-12 nm in diameter) encapsulated in PMMA NPs. The MNPsPMMA-FA obtained by miniemulsion polymerization presented a sub-micrometric size with a spherical morphology and unimodal size distribution. Other important factor in the preparation of NPs for biomedical application is the zeta potential, since particle size can influence their ability to interact with cells. At pH 7.4 the zeta potential of MNPsPMMA (−37 mV ± 4.8) and MNPsPMMA-FA

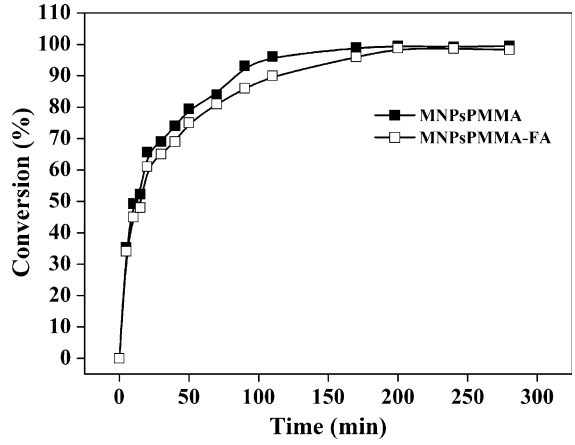


**Fig. 1** Gravimetric conversion analyses of the MNPsPMMA and MNPsPMMA-FA NPs obtained by miniemulsion polymerization

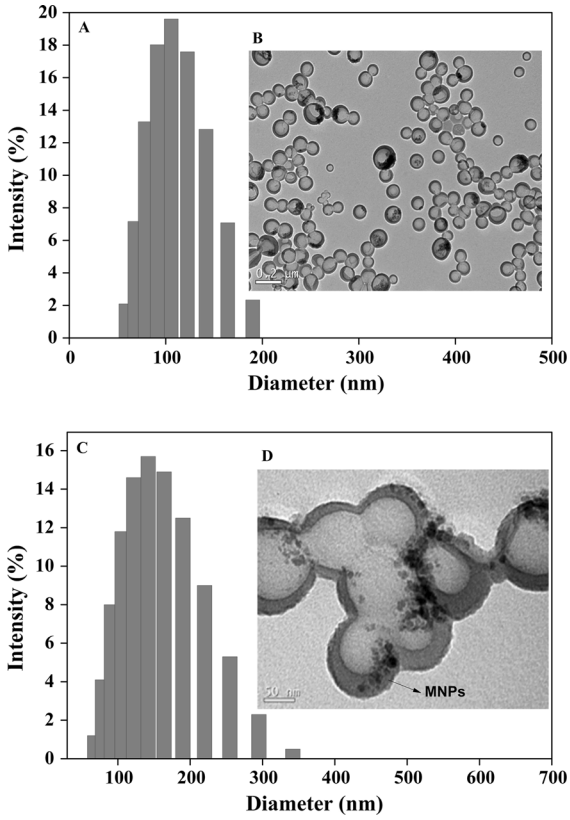


**Fig. 2** **a** and **c** dynamic light scattering; **b** and **d** transmission electron microscopy images of MNPsPMMA and MNPsPMMA-FA NPs, respectively. Data refer mean ± standard deviation ($n = 3$) different experiments

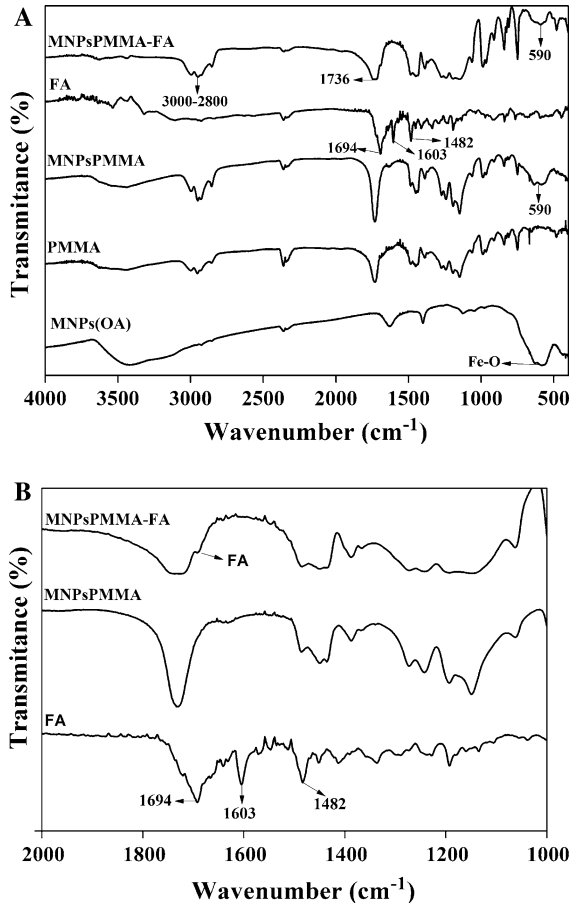


**Fig. 3** **a** FTIR spectrum: A MNPs(AO), PMMA, FA, MNPsPMMA and MNPsPMMA-FA and **b** FTIR spectrum at low scale: FA and MNPsPMMA-FA NPs

NPs (−38 mV ± 4.5) is not significantly different. The negative zeta potential can be attributed to the carboxylic groups of oleic acid and folic acid on the NPs surface. The high negative values of zeta potential are related to the good colloidal stability of NPs and their possible interactions with biological medium (He et al. 2010).

The FTIR analyses (Fig. 3) were performed, in order to evaluate possible chemical interactions of MNPs and FA on PMMA NPs. FTIR spectrum (Fig. 3a) showed a band at 1736 $cm^{-1}$ corresponding to C=O groups of PMMA. In addition, the bands in the 3000–2800 $cm^{-1}$ region are attributed to the stretching of C-H bonds of the saturated alkane in PMMA (Feuser et al. 2016). The peak at approximately 580 $cm^{-1}$ corresponds to asymmetric stretching vibrations of Fe–O ligands, which is attributed to the MNPs (Andhariya et al. 2013; Feuser et al. 2015a). The absorption bands at 1694 (amide I), 1603 (amide II) and 1482 $cm^{-1}$ (ring phenyl) are characteristic peaks of FA (Pan et al. 2013; Sahoo et al. 2013; Yoo et al. 2013; Duan et al. 2012; Zhang et al. 2007). The FTIR spectrum of MNPsPMMA-FA NPs suggested an adsorption of FA onto NPs due to the appearance of an additional band at 1694 $cm^{-1}$, as shown in Fig. 3b.

X-ray diffraction (XRD) patterns for the naked MNPs(OA) and MNPsPMMA-FA NPs are shown in Fig. 4. Figure 4 shows six characteristic peaks from the cubic inverse spinel structure of bulk magnetite/maghemite, observed at $2\theta = (220)$, (311), (400), (422), (511) and (440) (Dorniani et al. 2012; Yang et al. 2014). These results demonstrate that the MNPsPMMA-FA has the expected crystalline structure of magnetite/maghemite. An additional broad

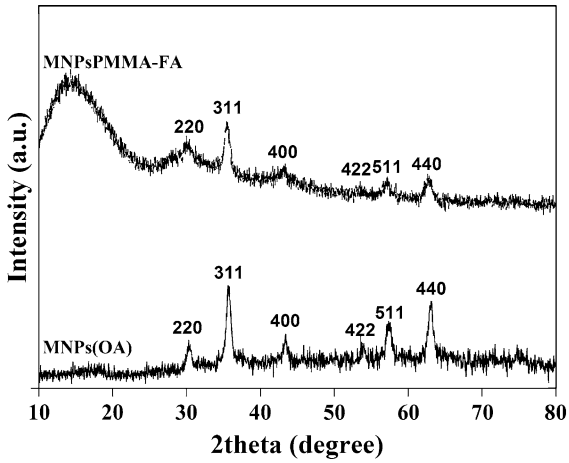


**Fig. 4** XRD powder diffraction patterns of MNPs(OA) and MNPsPMMA-FA NPs

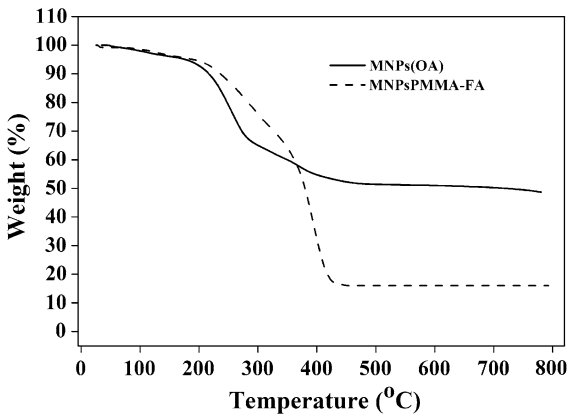


**Fig. 5** TGA analyses of MNPs(OA) and MNPsPMMA-FA NPs

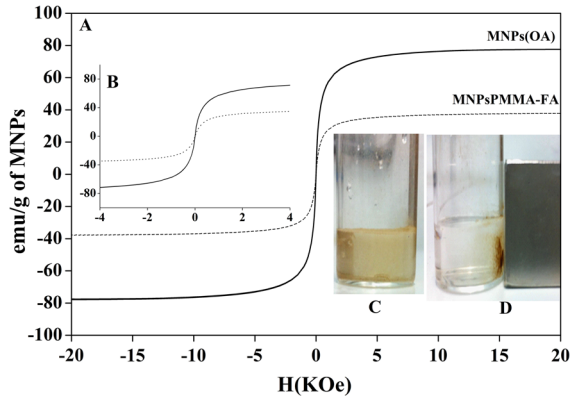


**Fig. 6** VSM analyses of magnetic properties of MNPs(OA) and MNPsPMMA-FA NPs with magnetic field of *a* 20 KOe and *b* 4 KOe. MNPsPMMA-FA NPs in PBS (7.4) *c* without application of an external magnetic field and *d* with application of an external magnetic field

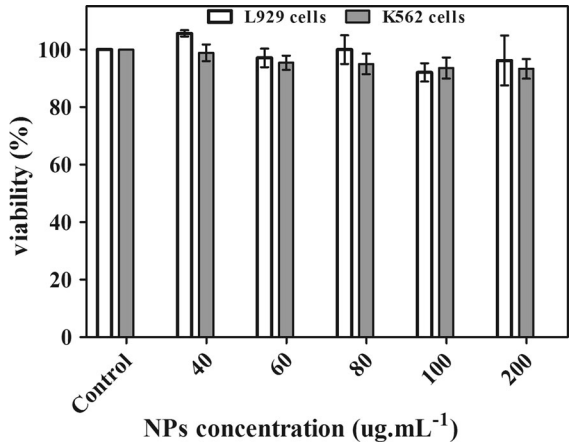


**Fig. 7** Cytotoxicity assay. Cytotoxicity effects of different concentrations of MNPsPMMA-FA on L929 and K562 cells exposed 24 h. The cell viability was monitored through MTT assay. ($p > 0.05$) using one-way ANOVA followed by post-test Bonferroni's

peak for the MNPsPMMA-FA NPs was observed at an angle between 10 and 20°, which are characteristic of amorphous polymers. (Feuser et al. 2015a; Feuser et al. 2016; Sahoo et al. 2013).

TGA analysis was performed estimating the total concentration of MNPs in formulation. Figure 5 shows mass loss in the temperature range from 20 to 220 °C, which can be attributed to the evaporation of water (Nan et al. 2013). The weight loss between 230 and 420 °C corresponds to the polymer PMMA, which are completely degraded when reaching approximately 410 °C, co-stabilizer (Crodamol); OA and FA contribute to the major portion of the total weight. (Landfester and Ramires 2003; Mohapatra et al. 2007; Feuser et al. 2015a). The residual weight of 16 % corresponds to the encapsulated MNPs.

The magnetic properties of MNPs(OA) and MNPsPMMA-FA NPs were ascertained by VSM (Fig. 6). The encapsulation of MNPs in PMMA NPs with FA-modified surface showed typical superparamagnetic behavior at room temperature (Fig. 6a, b), with the absence of hysteresis loop and a low remanent magnetization/saturation magnetization (Mr/Ms) ratio value, and a coercive field (Hc) of $5.0 \times 10^{-2}$ and 0.4, respectively (Chandrasekharana et al. 2011; Nan et al.

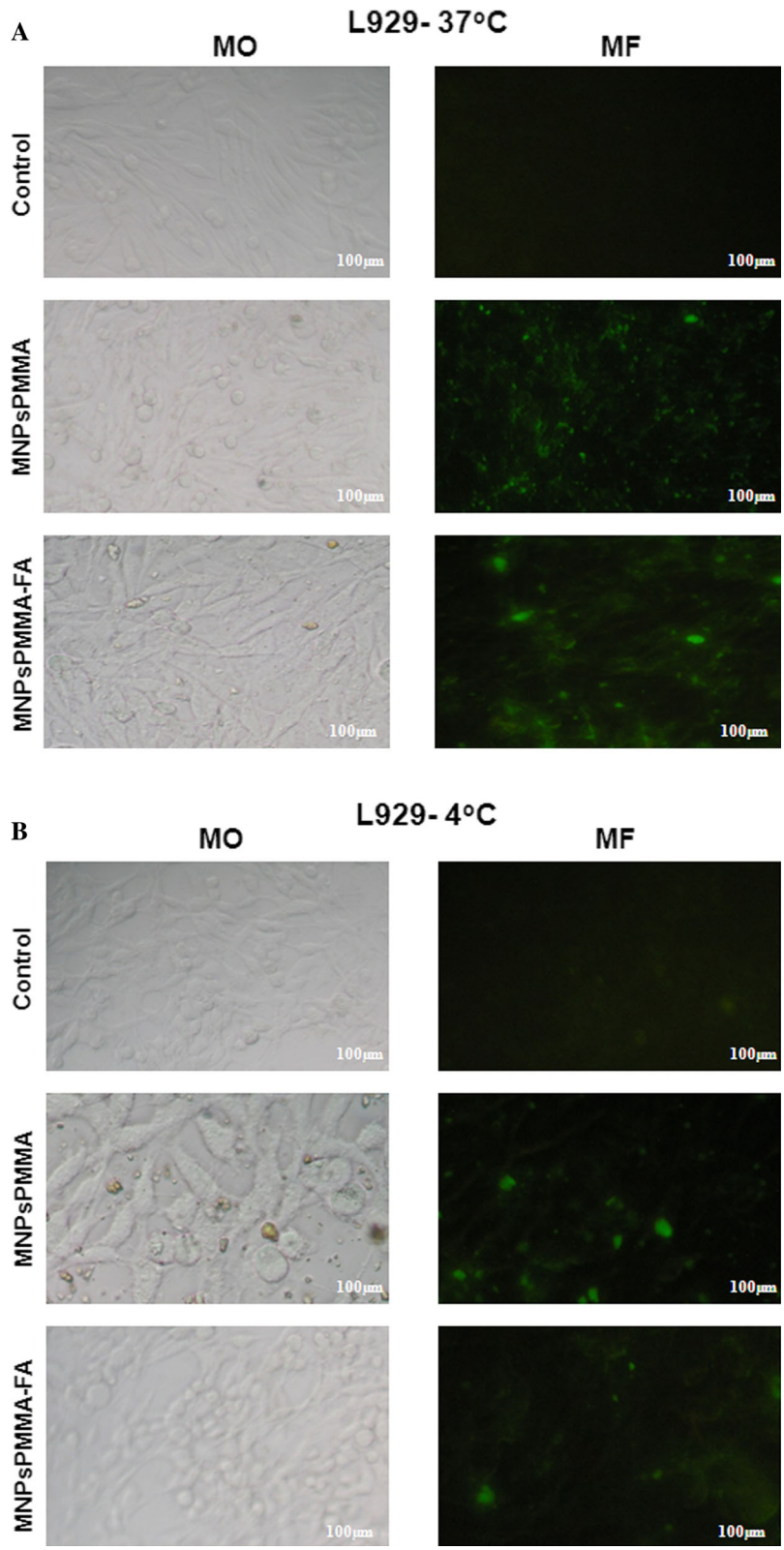


**Fig. 8** Optical (MO) and fluorescence (MF) microscopy images of L929 and K562 cells. The cells were treated with MNPsPMMA or MNPsPMMA-FA at concentration of 100 μg $mL^{-1}$ and incubated at 37 °C or at 4 °C for 2 h, after this period the cell morphology was evaluated by optical microscopy and the fluorescence of NPs was monitored by fluorescence microscopy (Olympus BX41)

**Fig. 8** continued

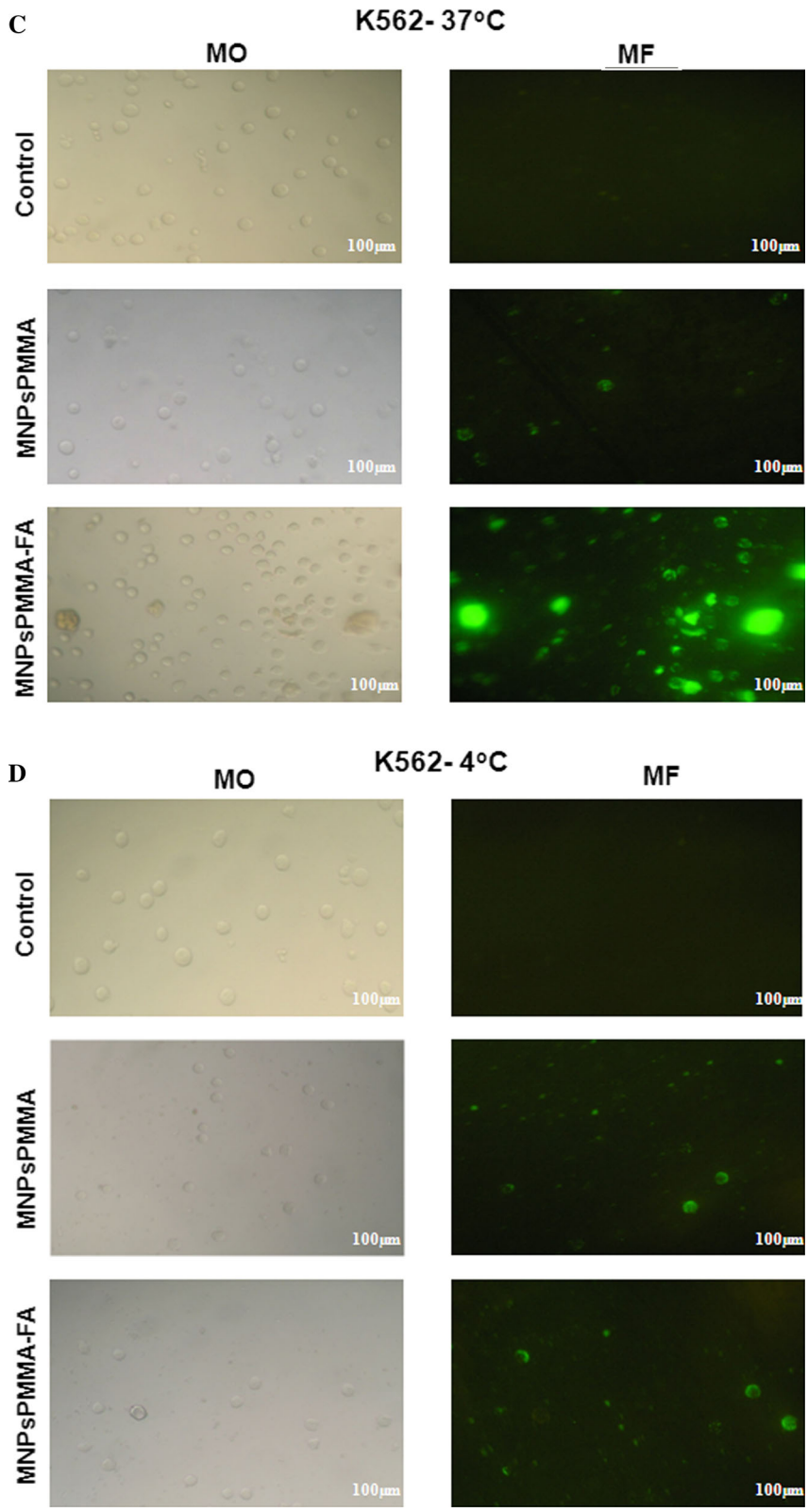

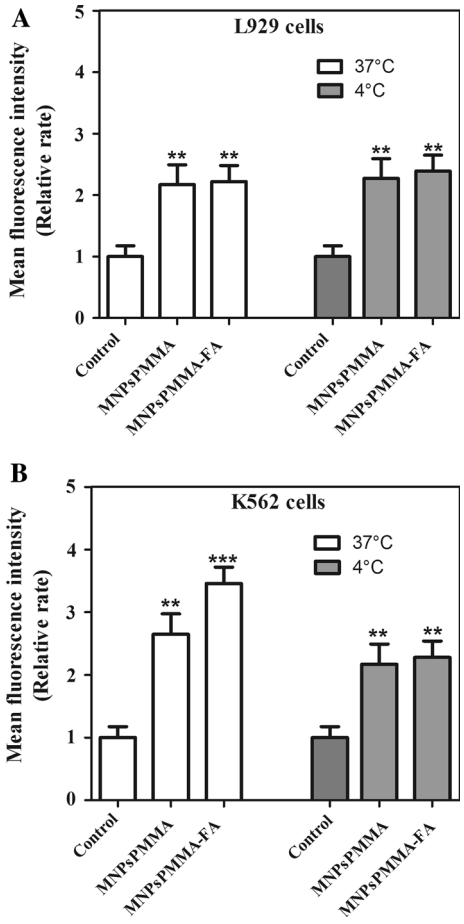


**Fig. 9** Quantification of mean fluorescence intensity by ImageJ software. Cells (K562 and L929) were incubated with MNPsPMMA and MNPsPMMA-FA NPs at 37 °C and 4 °C for 2 h, labeled with 6-coumarin at concentration of 100 μg $mL^{-1}$. $^{**}p < 0.001$, $^{***}p < 0.001$ compared to control groups, using one-way ANOVA followed by Bonferroni's post-test. *Scale bar* 100 μm

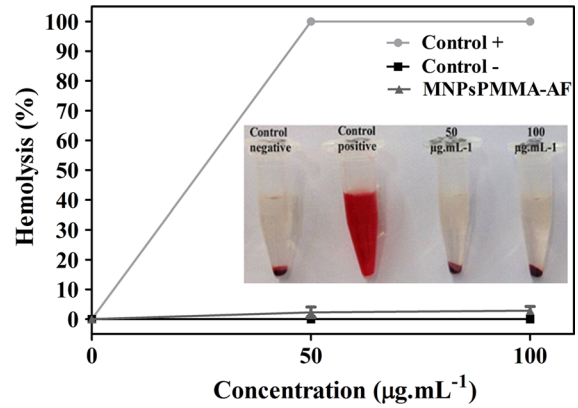


**Fig. 10** Hemolysis Assay of MNPsPMMA-FA. Relative rate of hemolysis in human RBCs upon incubation with MNPsPMMA-FA at concentration of 50 and 100 μg $mL^{-1}$. The presence of hemoglobin in the supernatant (*turbid*) was observed at 540 nm. Data are mean ± SD ($n = 3$)

2013; Mody et al. 2014; Yang et al. 2014). The superparamagnetic proprieties are very important for biomedical field. Thus, when an external magnetic field is not applied, their overall magnetization value is randomized to zero, avoiding the interactive behavior of the nanoparticles (Mody et al. 2014). The value of magnetization saturation (Ms) in emu/g of MNPs was obtained considering the iron oxide mass determined by TGA (Fig. 5). The Ms value was 37 and 66 emu/g for MNPsPMMA-FA NPs and MNPs(OA). The decrease in Ms value can be attributed to the dense coating of PMMA, as well as oxidation processes during the sonication, leading to the formation of some nonmagnetic or low Ms iron oxide, since maghemite (-$Fe_2O_3$) has a lower Ms of 60–80 emu/g compared to 92–100 emu/g for magnetite (Landfester and Ramires 2003; Chandrasekharana et al. 2011; Feuser et al. 2015b). However, this Ms value was enough to move encapsulated MNPs quickly and can be easily separated from the aqueous phase by the action of an external magnetic field gradient, which is shown in Fig. 6c, d. Hence, MNPsPMMA-FA NPs can be directed towards a specific target in the human body, with application of an external magnetic field.

To verify the cytotoxic effect of MNPsPMMA-FA NPs on L929 and K562 cells, the MTT assay was performed. As shown in Fig. 7, the MNPsPMMA-FA NPs did not significantly reduce cell viability ($p > 0.05$) on L929 cells at different concentrations (20, 40, 60, 80, and 100 ug $mL^{-1}$). These results are very important because they will facilitate innovative research of new nanomaterials for hyperthermia-based treatment and drug release systems. The non-cytotoxicity on L929 cells is important, since ISO 10993-5 recommends these cells for in vitro biocompatibility assays of new materials for biomedical application. The same results were observed when the cytotoxicity of MNPsPMMA-FA NPs was evaluated on K562 cells at different concentrations (40, 60, 80, 100 and 200 ug $mL^{-1}$of NPs/mL), as shown in Fig. 7.

Fluorescence microscopy assay was performed in order to evaluate the morphology and cellular uptake on

L929 (non-tumor) and K562 (tumor) cells overexpressing FR-β. The cells were treated with 13 ug $mL^{-1}$ of MNPsPMMA-FA and MNPsPMMA at two different temperatures (4 °C and 37 °C). As shown in Fig. 8, L929 and K562 cells incubated for 24 h at 37 and 4 °C, and did not present significant changes in their morphology. The cellular uptake assays showed a higher internalization of MNPsPMMA-FA than MNPsPMMA at 37 °C in K562 cells, which can be shown by their bright fluorescence (Fig. 8). These results were corroborated with the quantification of fluorescence, which showed a significant increase in fluorescence intensity of MNPsPMMA-FA when compared with MNPsPMMA. These increases in cellular uptake suggested that MNPsPMMA-FA entered into cancer cells by folate receptor-mediated endocytosis (Zheng et al. 2014; Kam et al. 2005; García-Días et al. 2011). On the other hand, when folate receptor-mediated endocytosis was blocked by low temperature at 4 °C, there was no significant difference in cellular uptake, as shown in Figs. 8 and 9. However, when L929 cells were used, similar results were observed for L929 cells at 37 and 4 °C (Figs. 8 and 9). These results were expected for L929 cells, since they do not express FR, suggesting that the NPs entered into cells by energy-independent mechanisms (Kam et al. 2005; Zheng et al. 2014). All endocytosis pathways are energy- and temperature-dependent mechanisms, which involve the uptake of NPs in small invaginations of membrane vesicles (Rastogi et al. 2014). Finally, our results showed that the superparamagnetic PMMA NPs with an FA modified surface are possibly an attractive target for cancer selective delivery by FR (Moriyama et al. 1986; Moulin et al. 2007; Wibowo et al. 2013; Van der Heijden et al. 2009; Qi and Ratnam 2006).

In order, to evaluate the biocompatibility on human red blood cells, hemolysis assays were carried out, which is shown in Fig. 9. The hemolysis assay is an important test to assess cytotoxicity in red blood cells (Chen et al. 2012; Zhou et al. 2011). According to the criterion of Standard Test Method for Analysis of Hemolytic Properties of Nanoparticles (ASTM E2524–08), a percentage hemolysis >5 % indicates that the test material causes damage. As shown in Fig. 10, high concentrations of MNPsPMMA-FA incubated for 24 h with human red blood cells did not exceed 5 %. The non-hemolytic character confirms the hemocompatibility of NPs obtained by miniemulsion polymerization, which can be an alternative for drug delivery systems administered systemically for leukemic treatment.

## Conclusion

The synthesis of surface modified superparamagnetic PMMA with FA obtained by miniemulsion polymerization resulted in a stable polymeric system in aqueous dispersion, with good polydispersity index and biocompatibility. MNPsPMMA-FA presented a significant increase in the K562 cell uptake at 37 °C, when compared with the MNPsPMMA, suggesting that it enters into cancer cells by folate receptor-mediated endocytosis. When the MNPsPMMA-FA was incubated at 4 °C, there was a reduction in cellular uptake, demonstrating that the mechanism of entering into K562 cells is energy dependent (endocytosis). The hemolysis assay demonstrated the hemocompatibility of MNPsPMMA-FA, which can be administered at 100 μg $mL^{-1}$ without causing any damage to human red blood cells. Moreover, other studies are being performed, such as, drug encapsulation for cancer treatment and cellular uptake assays to improve and understand the entering mechanism of these NPs in cells overexpressing FR-α and FR-β.

**Acknowledgments** We acknowledge Laboratório Central de Microscopia Eletrônica da UFSC (LCME-UFSC) and Laboratório Multiusuário de Caracterização Magnética de Materiais (LMCMM-UFSC) for TEM images and magnetization measurements. We are also grateful to Coordenação de Aperfeiçoamento de Pessoal de Nivel Superior, CAPES, and Conselho Nacional de Desenvolvimento Científico e Tecnológico, CNPq, for their financial support.

## References

Abulateefeh SR, Spain SG, Thurecht KJ, Aylott JW, Chan WC, Garnett MC, Alexander C (2011) Thermoresponsive polymer colloids for drug delivery and cancer therapy. Macromol Biosci 1:1722–1734. doi:10.1002/mabi.201100252

Akbarzadeh A, Samiei M, Davaran S (2012) Magnetic nanoparticles: preparation, physical properties, and applications in biomedicine. Nanoscale Res Lett 7(1):144. doi:10.1186/1556-276X-7-144

Andhariya N, Upadhyay R, Mehta R, Chudasama B (2013) Folic acid conjugated magnetic drug delivery system for controlled release of doxorubicin. J Nanopart Res 15:1416. doi:10.1007/s11051-013-1416-9

Arosio P, Orsini F, Piras AN, Sandreschi S, Chiellini F, Corti M, Masa M, Múčková M, Schmidtová L, Ravagli C, Baldi G,

Nicolato E, Conti G, Marzola P, Lascialfari A (2015) MR imaging and targeting of human breast cancer cells with folate decorated nanoparticles. RSC Adv 5:39760–39770. doi:10.1039/C5RA04880J

Asua JM (2014) Mapping the morphology of polymer-inorganic nanocomposites synthesized by miniemulsion polymerization. Macromol Chem Phys 215:458–464. doi:10.1002/macp.201300696

Bettencourt A, Almeida AJ (2010) Poly(methyl methacrylate) particulate carriers in drug delivery. J. Microencap. 29(4):353–367. doi:10.3109/02652048.2011.651500

Chandrasekharana P, Maity D, Yong CX, Chuangc KH, Ding J, Feng SS (2011) Vitamin E (D-alpha-tocopheryl-co-poly (ethylene glycol) 1000 succinate) micelles-superparamagnetic iron oxide nanoparticles for enhanced thermotherapy and MRI. Biomaterials 32(24):5663–5672. doi:10.1016/j.biomaterials.2011.04.037

Chen D, Tang Q, Li X, Zhou X, Zang J, Xue W-Q, Xiang J-Y, Guo C-Q (2012a) Biocompatibility of magnetic Fe3 O4 nanoparticles and their cytotoxic effect on MCF-7 cells. J Nanomed 7:4973–4985. doi:10.2147/IJN.S35140

Chen ML, He YJ, Chen XW, Wang JH (2012b) Quantum dots conjugated with $Fe_3O_4$-filled carbon nanotubes for cancer-targeted imaging and magnetically guided drug delivery. Langmuir 28:16469–16476. doi:10.1021/la303957y

Chen C, Ke J, Zhou XE, Yi W, Brunzelle JS, Li J, Eu-Leong Y, Xu HE, Karsten M (2013) Structural basis for molecular recognition of folic acid by folate receptors. Nature 500:486–489. doi:10.1038/nature12327

Chertok B, Moffat BA, David AE, Yu F, Bergemann C, Ross BD, Yang VC (2008) Iron oxide nanoparticles as a drug delivery vehicle for mri monitored magnetic targeting of brain tumors. Biomaterials 29:487–496. doi:10.1016/j.biomaterials.2007.08.050

Collins TJ (2007) ImageJ for microscopy. Biotechniques 43:S25–S30. doi:10.2144/000112517

Crespy D, Landfester K (2010) Miniemulsion polymerization as a versatile tool for the synthesis of functionalized polymers. Beilstein J Org Chem 6:1132–1148. doi:10.3762/bjoc.6.130

Dong S, Cho HJ, Lee WY, Roman M (2014) Synthesis and cellular uptake of folic acid-conjugated cellulose nanocrystals for cancer targeting. Biomacromolecules 15:1560–1567. doi:10.1021/bm401593n

Dorniani D, Hussein MZB, Kura AU, Fakurazi S, Shaari AH, Zalinah A (2012) Preparation of $Fe_3O_4$ magnetic nanoparticles coated with gallic acid for drug delivery. Int J Nanomed 7:5745–5756. doi:10.2147/IJN.S35746

Duan J, Liu M, Zhang Y, Zhao J, Pan Y, Yang X (2012) Folate-decorated chitosan/doxorubicin poly(butyl)cyanoacrylate nanoparticles for tumor-targeted drug delivery. J Nanopart Res 14:761–770

Fan L-H, Luo Y-L, Chen Y-S, Zhang C-H, Wei Q-B (2009) Preparation and characterization of Fe3O4 magnetic composite microspheres covered by a P(MAH-co-MAA) copolymer. J Nanopart Res 11:449–458. doi:10.1007/s11051-008-9556-z

Feuser PE, Bubniak LS, Santos-Silva MC, Cas Viegas A, Castilho-Fernandes A, Nele M, Ricci-Júnior E, Tedesco AC, Sayer C, Araújo PHH (2015a) Encapsulation of magnetic nanoparticles in poly(methyl methacrylate) by miniemulsion and evaluation of hyperthemia in U87MG cells. Europ J Polym 68:355–365. doi:10.1016/j.eurpolymj.2015.04.029

Feuser PE, Fernades AC, Nele M, Cas Viegas A, Tedesco AC, Ricci-Júnior E, Sayer C, de Araújo PHH (2015b) Simultaneous encapsulation of magnetic nanoparticles and zinc phthalocyanine in poly(methyl methacrylate) nanoparticles by miniemulsion polymerization and in vitro studies. Colloid Surf B 135:357–364. doi:10.1016/j.colsurfb.2015.07.067

Feuser PE, Gaspar PC, Jacques AV, Tedesco AC, Santos-Silva MC, Ricci-Júnior E, Sayer C, Araújo PHH (2016) Synthesis of ZnPc loaded poly(methyl methacrylate) nanoparticles via miniemulsion polymerization for photodynamic therapy in leukemic cells. Mater Eng C 60:458–466. doi:10.1016/j.msec.2015.11.063

García-Díaz M, Nonell S, Villanueva A, Stockert JC, Cañete M, Casadó M, Mora M, Sagristá ML (2011) Do folate-receptor targeted liposomal photosensitizers enhance photodynamic therapy selectivity? Biochim Biophys Acta 1808:1063–1071. doi:10.1016/j.bbamem.2010.12.014

Gosavi SS, Gosavi Y, Alla RK (2010) Local and Systemic Effects of Unpolymerised Monomers. Dent Res J (Isfahan) 7(2):82–87

Gupta AK, Gupta M (2005) Synthesis and surface engineering of iron oxide nanoparticles for biomedical applications. Biomaterials 25:3995–4021. doi:10.1016/j.biomaterials.2004.10.012

He L, Li Z, Fu J, Deng Y, He N, Wang Z, Wang H, Shi Z, Wang Z (2009) Preparation of SiO2/(PMMA/Fe3O4) from monolayer linolenic acid modified $Fe_3O_4$ nanoparticles via miniemulsion polymerization. J Biomed Nanotechnol 5(5):596–601. doi:10.1166/jbn.2009.1065

He C, Hu Y, Yin L, Tang C, Yin C (2010) Effects of particle size and surface charge on cellular uptake and biodistribution of polymeric nanoparticles. Biomaterials 31(13):3657–3666. doi:10.1016/j.biomaterials.2010.01.065

Higuchi WI, Misra J (1962) Physical degradation of emulsions via the molecular diffusion route and the possible prevention thereof. J Pharm Sci 51:459. doi:10.1002/jps.2600510514

International standard: Biological Evaluation of Medical Devices–Part 5 (1992) Tests for Cytotoxicity: in vitro methods. ISO 10993-5

Kam NWS, O'Connell M, Wisdom JA, Dai H (2005) Carbon nanotubes as multifunctional biological transporters and near-infrared agents for selective cancer cell destruction. Proc Natl Acad Sci 102(33):11600–11605. doi:10.1073/pnas.0502680102

Kumar CSSR, Mohamad F (2011) Magnetic nanomaterials for hyperthermia-based therapy and controlled drug reléase. Adv Drug Deliv Rev 63(9):789–808. doi:10.1039/c3ra47542e

Landfester K (2009) Miniemulsion polymerization and the structure of polymer and hybrid nanoparticles. Ang Chem 48:4488–4507. doi:10.1002/anie.200900723

Landfester K, Mailander V (2013) Nanocapsules with specific targeting and release properties using miniemulsion polymerization. Expert Opin Drug Deliv 10:593–609. doi:10.1517/17425247.2013.772976

Landfester K, Ramires LP (2003) Encapsulated magnetite particles for biomedical application J Phys Condes Matter 15:1345–1361. doi:10.1088/0953-8984/15/15/304

Leamon CP, Low PS (1991) Delivery of macromolecules into living cells: a method that exploits folate receptor endocytosis. Proc Natl Acad Sci 88(13):5572–5576

Lee SJ, Shim Y-H, Oh JS, Jeong Y-I, Park IK, Lee HC (2015) Folic-acid-conjugated pullulan/poly(DL-lactide-co-glycolide) graft copolymer nanoparticles for folate-receptor-mediated drug delivery. Nanoscale Res Letters 10:43. doi:10.1186/s11671-014-0706-1

Mahdavian AR, Ashjari M, Mobarakeh HS (2008) Nanocomposite particles with core-shell morphology. I. preparation and characterization of $Fe_3O_4$–Poly(butyl acrylate-styrene) particles via miniemulsion polymerization. J Appl Polym Sci 21:1242–1249. doi:10.1002/app.28729

Mody VV, Cox A, Shah S, Singh A, Bevins W, Parihar H (2014) Magnetic nanoparticle drug delivery systems for targeting tumor. Appl Nanosci 4:385–392. doi:10.1007/s13204-013-0216-y

Mohapatra S, Mallick SK, Kmaiti T, Ghosh SK, Pramanik P (2007) Synthesis of highly stable folic acid conjugated magnetite nanoparticles for targeting cancer cells. Nanotechnology 18:385102. doi:10.1088/0957-4484/18/38/385102

Moriyama Y, Narita M, Sato K, Urushiyama M, Koyama S, Hirosawa H, Kishi K, Takahashi M, Takai K, Shibata A (1986) Application of hyperthermia to the treatment of human acute leukemia: purging human leukemic progenitor cells by heat. Blood 67(3):802–804

Moulin M, Dumontet C, Arrigo A-P (2007) Sensitization of chronic lymphocytic leukemia cells to TRAIL-induced apoptosis by hyperthermia. Cancer Lett 250(1):117–127. doi:10.1016/j.canlet.2006.10.019

Nan A, Leistner J, Turcu R (2013) Magnetite–polylactic acid nanoparticles by surface initiated organocatalysis ring opening polymerization. J Nanopart Res 15:1869

Pan Y-J, Li D, Jin S, Wei C, Wu QY, Guo J, Wang CC (2013) Folate-conjugated poly(N-(2-hydroxypropyl)-methacrylamide-co-methacrylic acid) nanohydrogels with pH/redox dual-stimuli response for controlled drug release. 4:3545, doi: 10.1039/c3py00249g

Pengcheng D, Huiying Y, Jin Z, Peng L (2013) Folic acid-conjugated temperature and pH dual-responsive yolk/shell microspheres as a drug delivery system. J Mater Chem B 1:5298. doi:10.1039/c3tb20975

Qi H, Ratnam M (2006) Synergistic induction of folate receptor B by all-trans retinoic acid and histone deacetylase inhibitors in acute myelogenous leukemia cells: mechanism and utility in enhancing selective growth inhibition by antifolates. Cancer Res 66:5875–5882. doi:10.1158/0008-5472.CAN-05-4048

Qiu G, Wang Q, Wang C, Lau W (2007) Polystyrene/$Fe_3O_4$ magnetic emulsion and nanocomposite prepared by ultrasonically initiated miniemulsion polymerization. Ultrason Sonochem 14:55–61. doi:10.1016/j.ultsonch.2006.03.001

Rastogi V, Yadav P, Bhattacharya SS, Mishra AK, Verma N, Verma A, Pandit JK (2014) Carbon nanotubes: an emerging drug carrier for targeting cancer cells. J Drug Deliv doi:10.1155/2014/670815

Romio AP, Rodrigues HH, Peres A, Viegas ADC, Kobitskaya E, Ziener U, Landfester K, Sayer C, Araújo PHH (2013) Encapsulation of magnetic nickel nanoparticles via inverse miniemulsion polymerization. J Appl Polym Sci 129:1426–1433. doi:10.1002/app.38840

Sahoo B, Sanjana K, Devi P, Banerjee R, Maiti TK, Pramanik P, Dhara D (2013) Thermal and pH responsive polymer-tethered multifunctional magnetic nanoparticles for targeted delivery of anticancer drug. ACS Appl Mater Interfac 5:3884–3893. doi:10.1021/am400572b

Saltan N, Kutlu HM, Hür D, Izcan A, Ridvan S (2011) Interaction of cancer cells with magnetic nanoparticles modified by methacrylamido-folic acid. Int J Nanomed 6:477–484. doi:10.2147/IJN.S16803

Simioni AR, Primo FL, Rodrigues MMA, Lacava ZGM, Morais PC, Tedesco AC (2007) Binding and photophysical studies of biocompatible magnetic fluid in biological medium and development of magnetic nanoemulsion: a new candidate for cancer treatment. IEE Trans Magn 43(6):2459–2461. doi:10.1109/TMAG.2007.894126

Sudimack JBA, Lee RJ (2000) Targeted drug delivery via the folate receptor. Ad Drug Deliv Rev 41:147–162. doi:10.1016/S0169-409X(99)00062-9

Van der Heijden JW, Oerlemans R, Dijkmans BAC, Qi H, Van der Laken CJ, Lems WF, Jackman AL, Kraan MC, Tak PP, Ratnam M, Jansen G (2009) Folate receptor as a potential delivery route for novel folate antagonists to macrophages in the synovial tissue of rheumatoid arthritis patients. Arthritis Rheum 60:12–21. doi:10.1002/art.24219

Wang JJ, Liu K, Sung K, Tsai C, Fang JY (2009) Lipid nanoparticles with different oil/fatty ester ratios as carriers of buprenorphine and its prodrugs for injection. Eur J Pharm Sci 38(2):138–146. doi:10.1016/j.ejps.2009.06.008

Wibowo SA, Singh M, Reeder KM, Carter JJ, Kovach AR, Menga W, Ratnam M, Zhang F III, Dann CE (2013) Structures of human folate receptors reveal biological trafficking states and diversity in folate and antifolate recognition. Proc Natl Acad Sci USA 110(38):15180–15188. doi:10.1073/pnas.1308827110

Xu C, Su S (2013) New forms of superparamagnetic nanoparticles for biomedical applications. Adv Drug Deliv Rev 65:732–743. doi:10.1016/j.addr.2012.10.008

Yan F, Li J, Zhang J, Liu F, Yang W (2011) Preparation of $Fe_3O_4$/polystyrene composite particles from monolayer oleic acid modified Fe3O4 nanoparticles via miniemulsion polymerization. J Nanopart Res 11:289–296. doi:10.1007/s11051-008-9382-3

Yang H, Li Y, Li T, Xu M, Chen Y, Wu C, Dang X, Liu Y (2014a) Multifunctional core/shell nanoparticles cross-linked polyetherimide-folic acid as efficient Notch-1 siRNA carrier for targeted killing of breast cancer. Sci Rep 4:7072. doi:10.1038/srep07072

Yang Y, Guo X, Wei K, Wang L, Yang D, Lai L, Cheng M, Liu Q (2014b) Synthesis and drug-loading properties of folic acid-modified superparamagnetic $Fe_3O_4$ hollow microsphere core/mesoporous $SiO_2$ shell composite particles. J Nanop Res 16(2210):1–10. doi:10.1007/s11051-013-2210-4

Yu T, Malugin A, Ghandehari H (2011) Impact of silica nanoparticle design on cellular toxicity and hemolytic activity. ACS Nano 5(7):5717–5728. doi:10.1021/nn2013904

Zhang JL, Srivastava RS, Misra RDK (2007) Core-shell magnetite nanoparticles surface encapsulated with smart

stimuli-responsive polymer: synthesis, characterization, and LCST of viable drug-targeting delivery system. Langmuir 23(11):6342–6351. doi:10.1021/la0636199

Zhang J, Jiaxin L, Razavi FS, Mumin AM (2011) One-pot synthesis and characterization of rhodamine derivative-loaded magnetic core–shell nanoparticles. J Nanopart Res 13:1909–1916. doi:10.1007/s11051-010-9942-1

Zhao DL, Zhang HL, Zeng XW, Xia QS, Tang JT (2013) Inductive heat property of $Fe_3O_4$/polymer composite nanoparticles in an AC magnetic field for localized hyperthermia. Biomed Mater 1:198–201. doi:10.1088/1748-6041/1/4/004

Zheng W, Gao F, Gu H (2005) Magnetic polymer nanospheres with high and uniform magnetite content. J Magn Magn Mater 288:403–410. doi:10.1016/j.jmmm.2004.09.125

Zheng N, YinL Song Z, Ma L, Tang H, Gabrielson NP, Lu H, Cheng J (2014) Maximizing gene delivery efficiencies of cationic helical polypeptides via balanced membrane penetration and cellular targeting. Biomaterials 35:1302–1314. doi:10.1016/j.biomaterials.2013.09.090

Zhou Q, Zhang Z, Chen T, Guo X, Xhou S (2011) Preparation and characterization of thermosensitive pluronic F127-b-poly(caprolactone) mixed micelles. Colloid Surf B 86(1):45–47. doi:10.1016/j.colsurfb.2011.03.013